Supporting Information

A general route towards two-dimensional organic crystal-based functional fibriform transistors for wearable electronic textiles

*Lei Zheng, Cong Wang, Xinzi Tian, Xiaotao Zhang, Huanli Dong and Wenping Hu**

Mr. L. Zheng, Ms. C. Wang, X. Tian, Prof. X. Zhang, and W. Hu

Tianjin Key Laboratory of Molecular Optoelectronic Sciences, Department of Chemistry, School of Science, Tianjin University and Collaborative Innovation Center of Chemical Science and Engineering (Tianjin), Tianjin 300072, China

Prof. H. Dong and W. Hu

Beijing National Laboratory for Molecular Sciences, Key Laboratory of Organic Solids, Institute of Chemistry, Chinese Academy of Sciences, Beijing 100190, China

Prof. W. Hu

Joint School of National University of Singapore and Tianjin University, International Campus of Tianjin University, Binhai New City, Fuzhou 350207, China

E-mail: huwp@tju.edu.cn

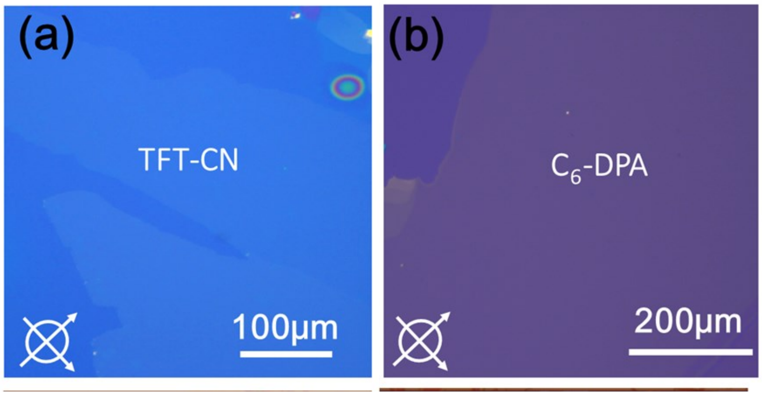

Fig. S1 a) and b) Polarized optical microscopy images of micrometer-sized TFT-CN and C_6-DPA 2DCOS on the SiO_2 (300 nm)/Si.

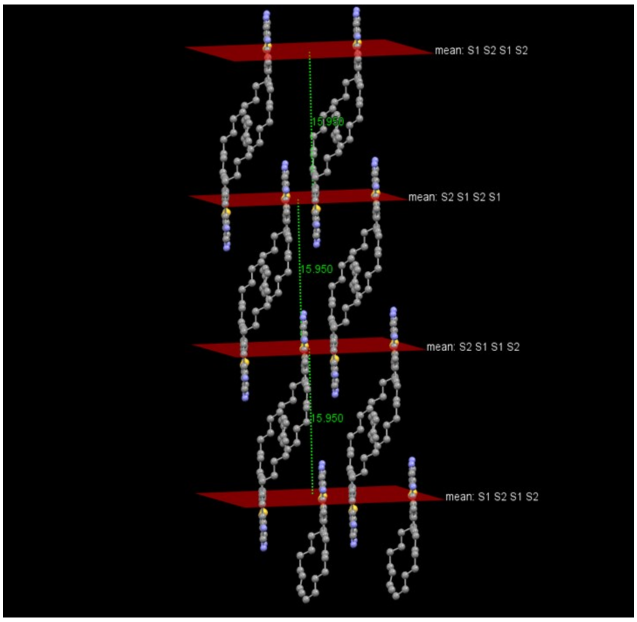

Fig. S2 The intermolecular distance of TFT-CN

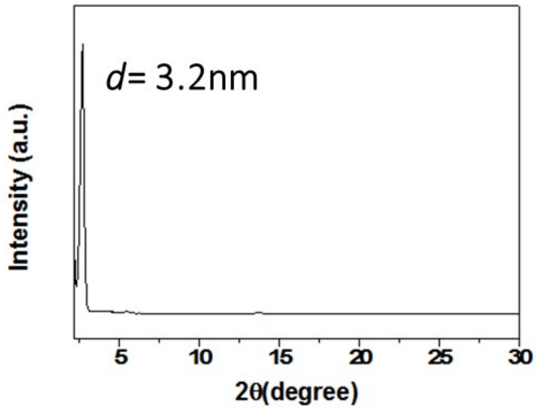

Fig. S3 XRD patterns of C_6-DPA which diffraction peaks at 2θ = 2.7°, 5.5°, and 13.5° were observed in. (The frst sharp diffraction peak corresponded to a *d*-spacing of ≈ 3.2 nm)

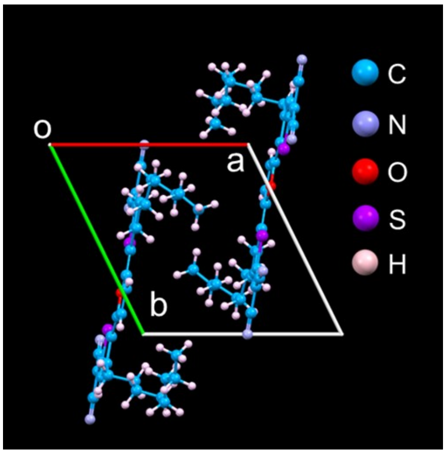

Fig. S4 The π–π interactions in TFT-CN crystal.

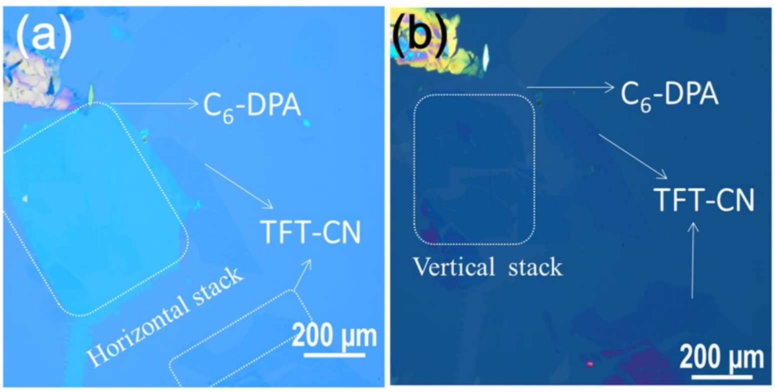

Fig. S5 The optical microscope (a) and crosspolarized microscope images (b) of TFT-CN and C_6-DPA 2DCOS with different stacking ways.

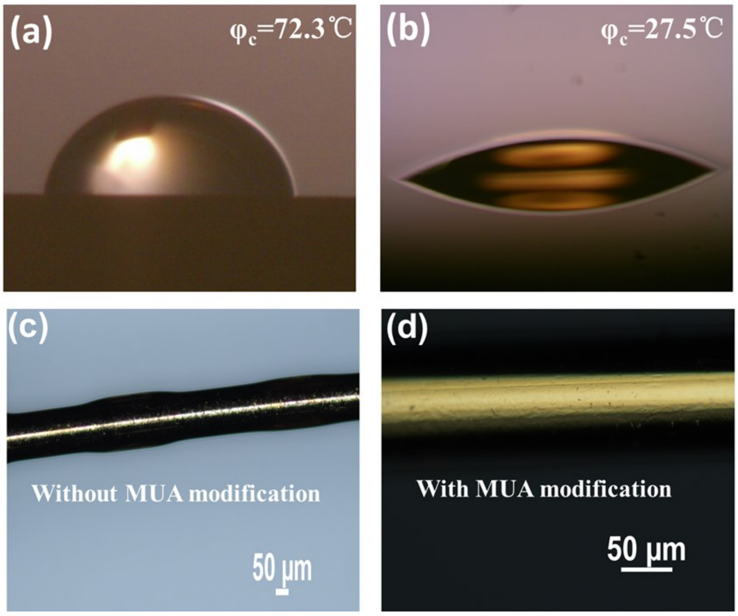

Fig. S6 a, b) The contact angle of bare Au and MUA modified Au. c-e) The Optical microscopy image of Au wire dip-coated PMMA layer. f) The Optical microscopy image of MUA modified wire with PMMA layer.

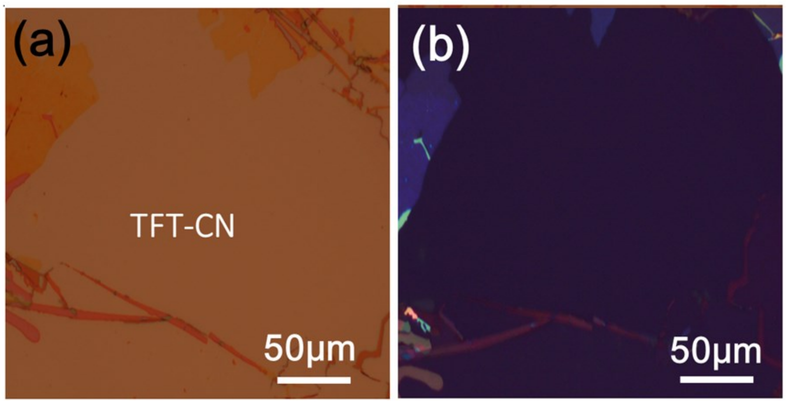

Fig. S7 The optical microscope (a) and crosspolarized microscope images (b) of 2DCOS on the PMMA/Au flexible substrate.

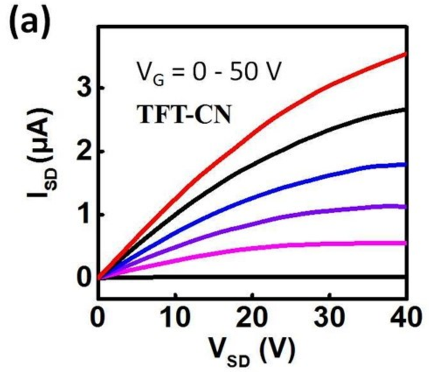

Fig. S8 a, b) The typical output curves of the fiber-shaped OFETs based on TFT-CN and C6-DPA 2DCOS.

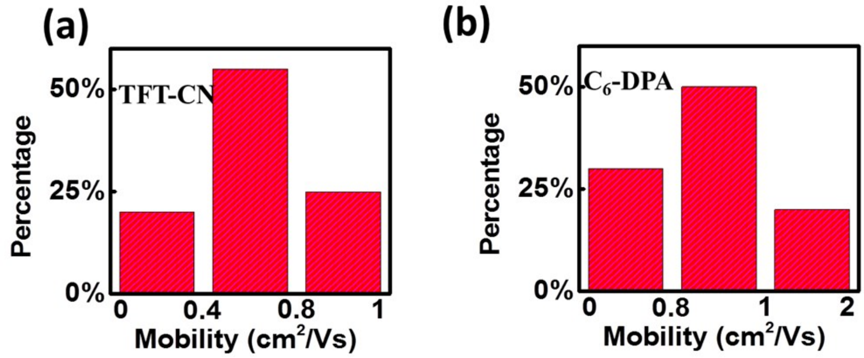

Fig. S9 Mobility distributions based on 30 devices (a) TFT-CN, (b) C_6-DPA.

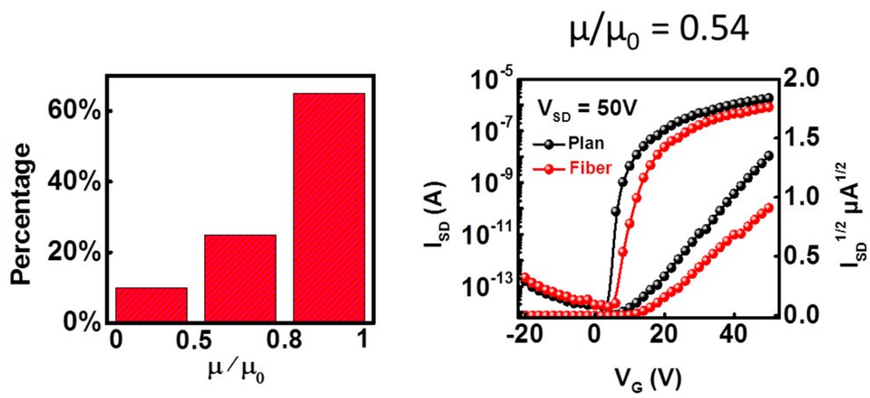

Fig. S10 a) The variations of mobilities between the before and after transferred devices based on these 30 TFT-CN devices. b) The typical transfer curves of the before and after transferred TFT-CN device.

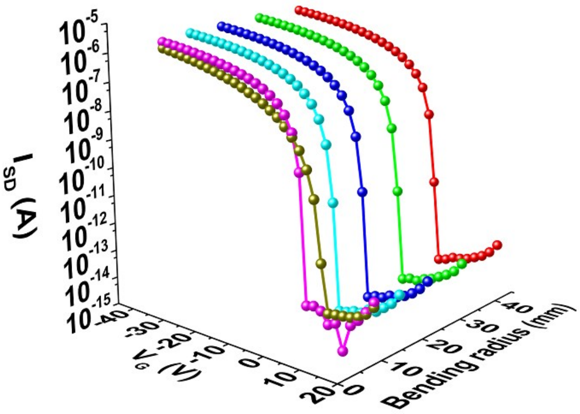

Fig.S11 The transfer characteristics plotted against the bending radius of the TFT-CN 2DCOS-based OFET.

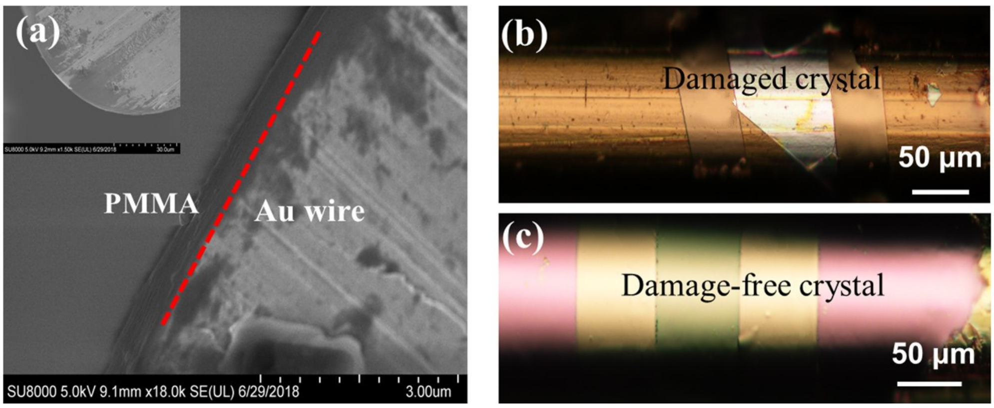

Fig. S12 a) The SEM image of a MUA-modified Au microfiber with 780-nm PMMA layer. b) Bottom-gate/top-contact (BGTC) device fabricated by a traditional method. c) Bottom-gate/top-contact (BGTC) device fabricated by jigsaw puzzle method.

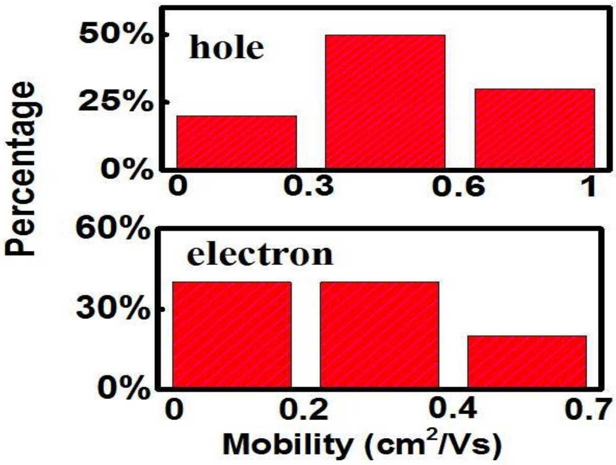

Fig. S13 Mobility distributions of ambipolar p-n junction devices based on 10 devices.

Table S1. Reported high performance ambipolar OFETs based on organic single-crystalline double component.

Type	p-type material	n-type material	Hole mobility ($cm^2V^{-1}s^{-1}$)	Electron mobility ($cm^2V^{-1}s^{-1}$)	Ref
Cocrystal	DPTTA	C_{60}	0.3	0.01	1
Cocrystal	4M-DSB	CN-TFPA	0.0067	0.67	2
Lateral junction	Dif-TES-ADT	BPE-PTCDI	0.32	0.43	3
Bilayer	C_8-BTBT	C_{60}	0.16	0.17	4
Bilayer	TIPS-PEN	PTCDI- C_8	0.23	0.13	5
Bilayer	C_6-DPA	TFT-CN	0.87	0.82	6
Bilayer	C_6-DPA	TFT-CN	0.9	0.65	**This work**

1. J. Zhang, J. Tan, Z. Ma, W. Xu, G. Zhao, H. Geng, C. a. Di, W. Hu, Z. Shuai, K. Singh and D. Zhu, Fullerene/sulfur-bridged annulene cocrystals: two-dimensional segregated heterojunctions with ambipolar transport properties and photoresponsivity, *J. Am. Chem. Soc.,* 2013, **135**, 558-561.
2. S. K. Park, S. Varghese, J. H. Kim, S.-J. Yoon, O. K. Kwon, B.-K. An, J. Gierschner and S. Y. Park, Tailor-made highly luminescent and ambipolar transporting organic mixed stacked charge-transfer crystals: an isometric donor–acceptor approach, *J. Am. Chem. Soc.,* 2013, **135**, 4757-4764.
3. X. Zhang, J. Mao, W. Deng, X. Xu, L. Huang, X. Zhang, S. T. Lee and J. Jie, Precise patterning of laterally stacked organic microbelt heterojunction arrays by surface–energy–controlled stepwise crystallization for ambipolar organic field–effect transistors, *Adv. Mater*., 2018, **30**, 1800187.

4. C. Fan, A. P. Zoombelt, H. Jiang, W. Fu, J. Wu, W. Yuan, Y. Wang, H. Li, H. Chen and Z. Bao, Solution–grown organic single–crystalline p–n junctions with ambipolar charge transport, *Adv. Mater,.* 2013, **25**, 5762-5766.
5. H. Shim, A. Kumar, H. Cho, D. Yang, A. K. Palai and S. Pyo, Laterally-stacked, solution-processed organic microcrystal with ambipolar charge transport behavior, *ACS Appl. Mater. Interfaces,* 2014, **6**, 17804-17814.
6. X. Zhu, Y. Zhang, X. Ren, J. Yao, S. Guo, L. Zhang, D. Wang, G. Wang, X.Zhang, R. Li and W.Hu, 2D molecular crystal bilayer p–n junctions: a general route toward high–performance and well–balanced ambipolar organic field–effect transistors, *small,* 2019, **15**, 1902187.

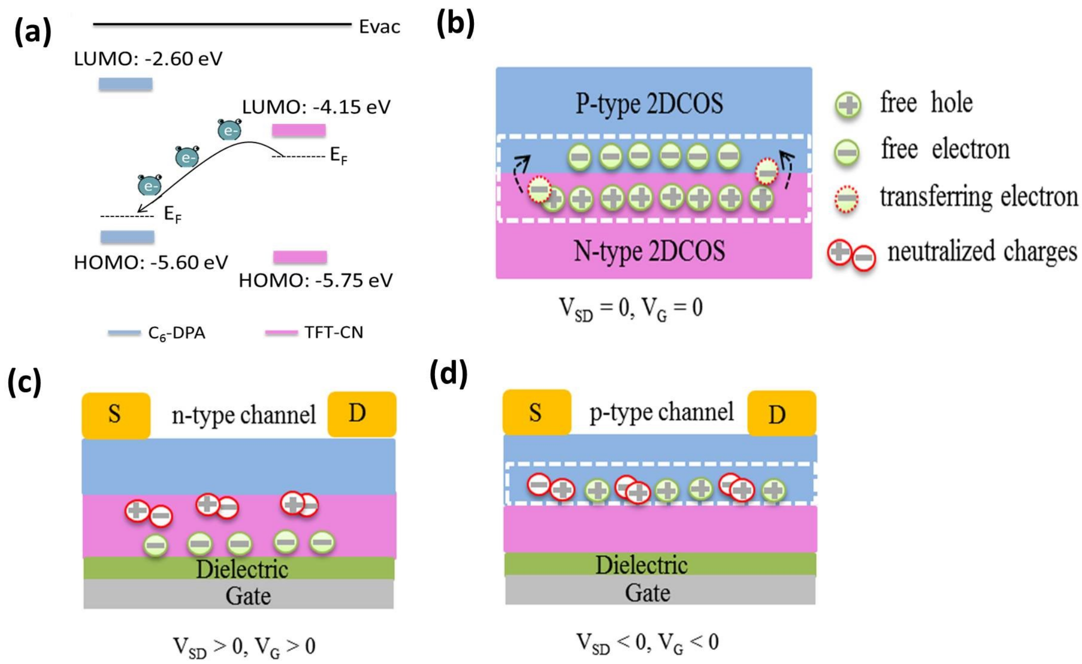

Fig. S14 The charge transport mechanism of bilayer 2DCOS-based p–n junction. a) Energy level alignment of C_6-DPA and TFT-CN. b-d) schematic illustrations of electron accumulation and hole accumulation modes of the ambipolar OFETs based onbilayer p–n junctions.

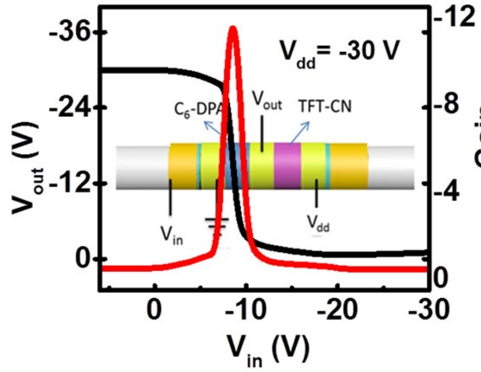

Fig. S15 Representative static voltage-transfer characteristics of the fibriform inverter with voltage gain operating under -30 V.

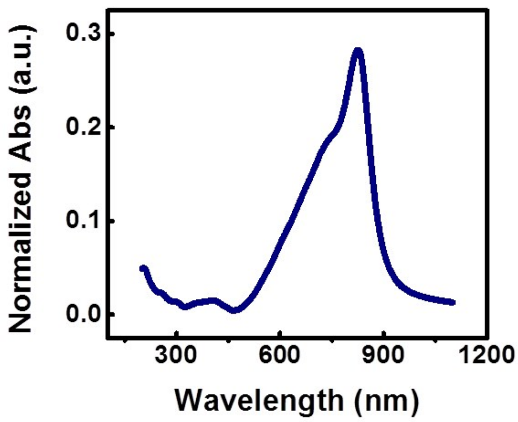

Fig.S16 The absorption spectrum of the TFT-CN film

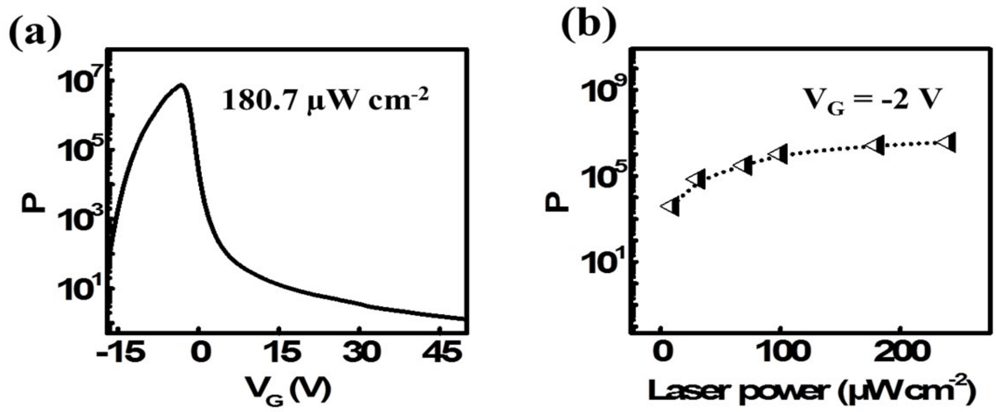

Fig. S17 The *P* of the fibriform phototransistors as a function of (a) V_G and (b) illumination intensity.

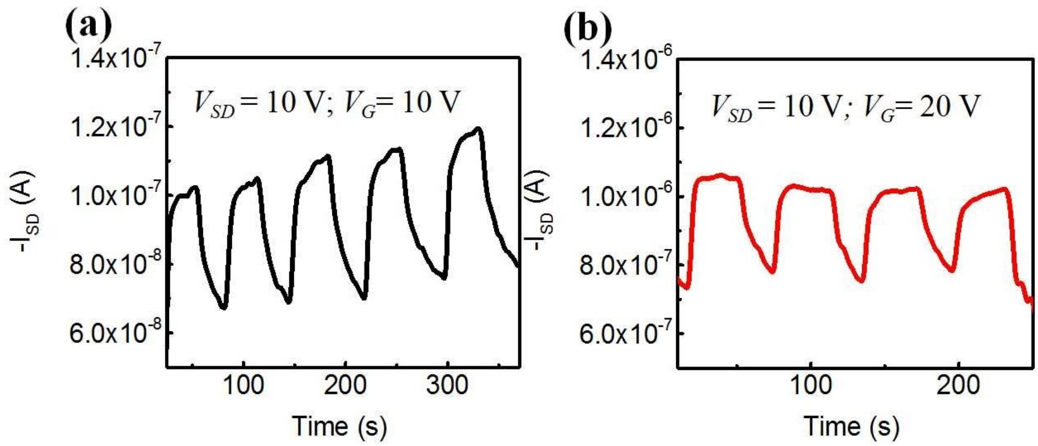

Fig. S18 Photoswitch of the fibriform NIR phototransistor operated at V_G = 10 V, V_{SD} = 10 V and V_G = 20 V, V_{SD} = 10 V based on an illumination intensity of 180.7 P.